

Article

Performance Analysis of a Compressor Rotor Dedicated to Low-Power Drive Systems

Natalia Kapela * , Karolina Wyzkiewicz and Andrzej Frąckowiak * Institute of Thermal Engineering, Poznan University of Technology, 60-965 Poznan, Poland;
karolina.wyzkiewicz@put.poznan.pl

* Correspondence: natalia.kapela@put.poznan.pl; (N.K.); andrzej.frackowiak@put.poznan.pl (A.F.)

Abstract: This study investigates the efficiency evaluation of a compressor rotor designed for drive units requiring compressors with a power demand of less than 30 kW. The primary aim of the research presented in this article is to assess the feasibility of utilizing axial compressors to maintain high efficiency across a broad range of rotor speeds. A critical challenge in the considered power range is the occurrence of low Reynolds numbers, specifically those below 250,000. This research seeks to identify the underlying causes of efficiency degradation at low Reynolds numbers and determine the rotor's geometric parameters which most significantly influence the localized efficiency drop. Compressor efficiency was evaluated through numerical simulations. The numerical model was validated using experimental data and subjected to a grid independence study. Simulations were conducted for nine geometric configurations of the axial compressor rotor, with modifications to parameters such as the blade angle, blade thickness, blade solidity, and hub-to-tip ratio. For each configuration, a series of simulations was performed at rotor speeds ranging from 400 RPM to 2400 RPM. The simulation results indicated that the blade angle solidity was the most influential parameter affecting efficiency. A reduction in the blade angle led to approximately a 20% decrease in efficiency, primarily due to localized flow separation near the blade tip. Additionally, altering the number of blades caused a 20% efficiency reduction attributed to hub corner separation. The findings enabled the identification of optimal parameters, which will serve as a foundation for efficiency testing in the multistage configuration.

Keywords: turbomachinery; axial compressor; Reynolds number



Academic Editor: Roberto Finesso

Received: 13 November 2024

Revised: 20 December 2024

Accepted: 27 December 2024

Published: 31 December 2024

Citation: Kapela, N.; Wyzkiewicz, K.; Frąckowiak A. Performance Analysis of a Compressor Rotor Dedicated to Low-Power Drive Systems. *Energies* **2025**, *18*, 123. <https://doi.org/10.3390/en18010123>

Copyright: © 2024 by the authors. Licensee MDPI, Basel, Switzerland. This article is an open access article distributed under the terms and conditions of the Creative Commons Attribution (CC BY) license (<https://creativecommons.org/licenses/by/4.0/>).

1. Introduction

1.1. Research Background

As a result of climate change and rising average annual temperatures, the demand for air conditioning systems is steadily increasing. Furthermore, the diversification of heat sources has contributed to a growing number of consumers opting to install heat pumps for heating purposes, often due to limited access to hot water and central heating systems. Air conditioning systems account for approximately 50% of the total energy consumption in commercial buildings [1–4]. In Europe, this figure rises to 53% for commercial buildings and 64% for residential buildings [5]. Consequently, improving the efficiency of any component within these systems is critical to reducing overall energy consumption. Various strategies are employed to enhance the efficiency of air-conditioning systems by increasing the coefficient of performance (COP). These strategies include adjusting the compressor speed [6,7], optimizing the working fluid within the heat exchanger [4,8], improving compressor cooling techniques [9], and utilizing ejectors as expansion devices [9,10].

1.2. Motivation: Industry Project

The motivation for this research stemmed from collaboration with industries on a project entitled ‘Development and demonstration of air conditioning and heating device based on turbomachinery without the use of harmful working agents’. The project focused on designing a compressor-turbine system integrated with a high-efficiency heat exchanger operating at a pressure of 1.5 bar. It was assumed that the polytropic efficiency of the flow machines would exceed 95%. To meet the stringent requirement of achieving such high efficiencies—particularly challenging for compression machines—a three-stage axial compressor was selected for design. Design constraints, including rotor size limitations, a predefined mass flow rate, and power demand, necessitated a flow kinematics framework with velocity values corresponding to a Reynolds number of 150,000 at the design point. This represents a relatively low Reynolds number for axial compressors and poses a significant design challenge.

The aforementioned project provided the impetus for scientific research into the flow and optimization of devices operating at low Reynolds numbers. Despite initial concerns about flow performance under conditions where the Reynolds number is relatively low, the developed device exhibited high efficiency. Through a comprehensive design process, a compressor (Figure 1) was created, achieving notable single-stage efficiencies of 97% in numerical simulations and 86% in experimental tests. As the axial compressor designed for the project utilized NACA65 profiles, it became clear that these profiles hold significant potential for application in axial compressor rotors dedicated to low-power systems (less than 30 kW). The research presented in this article builds on and expands this work, providing a more detailed analysis of the influence of various geometrical parameters on flow efficiency under low Reynolds number conditions.

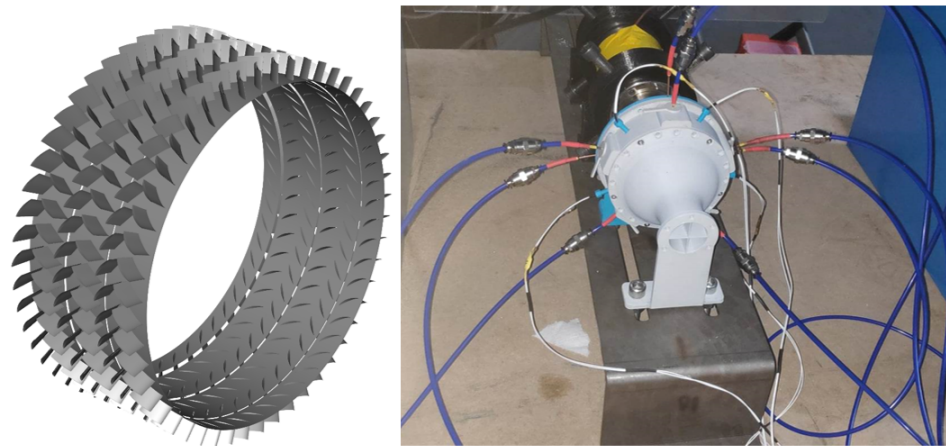


Figure 1. Axial compressor geometric model and experimental set-up (courtesy of APGAZ Company, Tempe, AZ, USA).

1.3. Literature Review

The compressor unit serves as the driving component of heat pump and air-conditioning systems. The power requirement of the compressor directly impacts the overall efficiency of the system. Higher compressor efficiency reduces the power required to achieve the desired heat output, thereby minimizing energy losses. The demand for low-power compressors is particularly evident in systems utilizing combustion, especially in cases where an increase in air or gas pressure is needed prior to the combustion process, but with a lower energy demand. Such solutions are commonly implemented in compact heating appliances, gas boilers, small combustion engines, smaller-scale industrial

combustion systems, and limited afterburning systems. The power consumption of the compressor is directly proportional to both the cooling capacity and the system's efficiency. The coefficient of performance (COP) (Equation (1)), defined as the ratio of cooling capacity to electrical power input, provides a useful metric for estimating this consumption:

$$\text{Compressor power [kW]} = \frac{\text{Cooling Capacity [kW]}}{\text{COP}} \quad (1)$$

In the context of small-scale industrial air-conditioning systems, the power output of the compressor typically ranges from 1.5 kW to 15 kW. This depends on the cooling demand and the overall efficiency of the system. Most air-conditioning systems are equipped with scroll, centrifugal, or inverter-type rotary compressors [11–18], with the majority operating within a heat output range from 3.5 kW [18] to 18 kW [12].

The application of axial compressors in air-conditioning systems presents a promising and potentially fruitful avenue for research. Axial compressors are inherently compact, especially when compared with centrifugal compressors that achieve the same flow rate and pressure ratio. If miniaturized, they could lead to the development of more compact air-conditioning systems. In scenarios where a high flow rate is needed or efficiency gains can be achieved through the use of advanced materials or technological improvements, an axial compressor may outperform traditional compressors in certain applications. Research into advanced materials, 3D printing, and nanotechnology has the potential to reduce the cost and complexity of axial compressors. For instance, the use of lightweight materials and novel manufacturing methods could make axial compressors more viable for integration into smaller, high-efficiency heating, ventilation, and air-conditioning (HVAC) systems in the future.

Most of the current and recent research has focused mainly on high-performance axial compressors where Mach numbers exceed 0.4, which corresponds to Reynolds numbers in excess of 500,000. These studies [19–21] have shown that maintaining a high compressor stage load is a key parameter for achieving higher efficiencies. However, increasing the load also leads to a significant increase in profile losses [22] and intensification of the hub corner separation [23]. Theoretically, an increase in efficiency can be achieved by reducing the global speed range.

Low Reynolds number (Re) conditions lead to higher viscous losses and reduced flow turning, significantly impacting compressor performance [24]. A low Re causes flow separation on the suction surface and boundary layer thickening, which diminishes the static pressure rise and increases the total pressure loss. Research conducted in [25,26] showed that in the range of Reynolds numbers smaller than approximately 60,000, the total pressure loss increases significantly [25,26].

The performance of axial compressors is closely related to their rotational speed, and the type of instability they experience is also directly associated with the speed [27,28]. At low speeds, axial compressors are more prone to rotating stalls, which can lead to a significant reduction in their operating range and efficiency [27–29]. To address this issue, researchers have explored various design strategies and flow control techniques to enhance the stability and performance of axial compressors in a small speed range. The coupling of variable frequency speed regulation and inlet guide vane-stator regulation can significantly improve the pressure ratio and efficiency of compressors under off-design conditions [27]. The latest research on axial compressor design for small speed ranges has focused on enhancing the stability, efficiency, and operating range through innovative blade designs, flow control techniques, and advanced modeling and optimization approaches [27,30–33].

The research presented in this article aims to explore the potential of using this type of compressor in drive systems requiring lower power compression than 30 kW. The considered power range assumes gas flows with mass flow rates of approximately 4 kg/s,

where a compressor stage with a pressure ratio of 1.08 would consume roughly 26 kW of power. The resulting pressure ratio could be achieved through the use of multistage variants, which would, of course, increase power demand. The subject of the study is an axial compressor rotor with similar parameters to those mentioned above. The research assumes that the designed rotor is typically the first stage of such a compressor, which usually has the lowest efficiency [34] due to reduced flow stability and a decreased pressure rise caused by the ‘entrance effect’. For subsequent stages of the multistage compressor, the incoming air is characterized by higher stability, which consequently increases its efficiency.

Numerical studies focus on optimizing the geometry of the compressor rotor, specifically examining which of the most important geometric parameters of the rotor have the greatest impact on the rotor efficiency. The research described in this article does not evaluate the efficiency of a full multistage compressor variant, as these are future studies. Before work on a multistage machine begins, it is essential to understand the design parameters. A review of the literature indicates that for high power ranges, the optimal values for parameters such as the blade solidity, blade angle, and HT are well established. However, these compressors operate in a higher Reynolds number range where compressors are subject to higher loads and greater flow stability due to high speeds. The authors chose to examine the behavior of the compressor as these parameters change in a lower speed range, where there are smaller aerodynamic loads and the flow field is less stable. The trends in flow behavior identified in this study will inform further research into optimizing the operation of the entire stage as well as the performance of the compressor in a multistage system.

2. Methods

2.1. Experimental Set-Up

In order to ascertain the validity of the numerical model, one of the geometric cases subjected to experimental testing in the NACA publication [35] was selected to validate the compressor rotor. NACA data are frequently used to validate numerical schemes, particularly in preliminary studies aimed at developing new flow machine designs or investigating the relevance of secondary phenomena. This is because the data are openly available and have been repeatedly verified as valid [36,37].

The experimental tests were conducted using a subsonic wind tunnel, the detailed configuration of which can be found in the aforementioned publication. The compressor tests were primarily based on pressure and mass flow rate measurements in the test section at a distance of 3.81 cm in front of the rotor. In order to minimize the impact of the rotor-mounted rake on the measuring instrument, the pressure-measuring tube was positioned at a distance of 10.16 cm from the rotor outlet. The pressures were gauged using altitude alcohol pressure manometers. The compressor was driven by a 55 kW direct-current motor capable of operation between 0 and 3600 RPM. The pressures and velocities were recorded over a speed range of 400–2400 RPM. Following each test, the flow measurement instruments were calibrated in a dedicated calibration tunnel. The static pressure calibration factors yielded results that were within 1/4 of a percent of the dynamic pressure. The tachometer utilized in the measurements was evaluated with the aid of a stroboscope, and its measurement error was determined to be 5 RPM, which corresponds to an error of 0.5% from the range of measurement speeds tested. The pressure reading was found to be accurate to within 0.03 cm of the alcohol column, which corresponds to an error of 0.1% expressed in terms of dynamic pressure under averaged measuring conditions. A comprehensive examination of the sources of error can be found in [35].

2.2. Reference Case Description

The rotor geometry for the reference case was reconstructed based on sourced data (Figure 2) [35]. The compressor rotor comprised 26 blades with profiles derived from the NACA65-(CL)10 series, based on known lift coefficient values at each radial section. Table 1 shows the geometric configuration of the base rotor. The rotor diameter was approximately 0.5 m at the hub and 0.77 m at the tip. The chord maintained a constant value along the radius, with a length of approximately 0.07 m. The blade solidity at the pitchline was 1.0, and the case where the blade angle (corresponding to the angle of attack) was 64.2 degrees above the design value has been validated.

The kinematics and thermodynamic parameters of the air at the compressor rotor inlet could be reconstructed thanks to the compressor inlet pressure and temperature values given in the publication (1.013 bar and 270 K, respectively) and a design coefficient quantity of 0.438. A rotor blade was constructed based on five profiles derived from the NACA65 series (Table 1). Based on the available data, it was calculated that the estimated compressor rotor power was 33 kW at a mass flow rate of 8.78 kg/s and 4.15 kW at a mass flow rate of 4.39 kg/s. These values correspond to the power demand values in the considered power range of air-conditioning systems. The Reynolds number range of the tests considered spanned from 40,000 (at 400 rpm) to 240,000 (at $n = 2400$ rpm), which aligns with the range of Reynolds numbers considered in this article.

Table 1. Design values for the base compressor rotor [35].

Radius Location	Profile	α (deg)	β_1 (deg)	ξ (deg)	σ	D/D_t
root	65-(13.5)10	15.60	48.9	24.2	1.135	0.784
inboard	65-(12)10	13.3	51.1	19.9	1.051	0.849
pitch	65-(11)10	12	52.5	17.5	1	0.892
outboard	65-(10)10	10.8	53.8	15.5	0.954	0.935
tip	65-(8.5)10	8.9	55.6	13	0.892	1

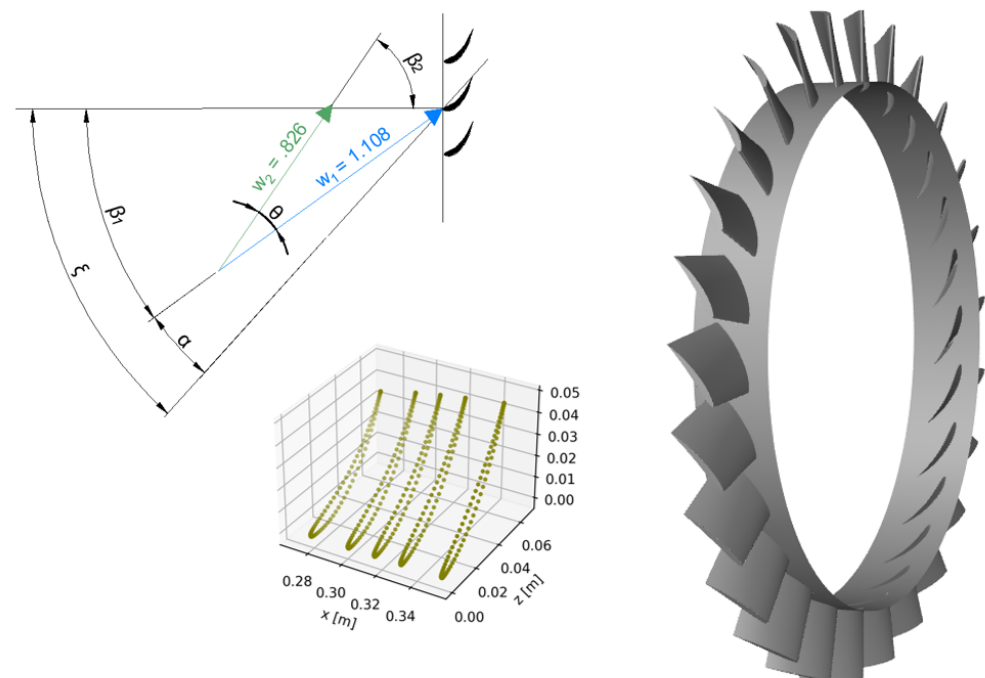


Figure 2. Selected parameters for flow kinematics (expressed in parts of tip velocity) and a view of the rotor geometry for the reference (distribution of profiles across radius and rotor view) case [35].

2.3. Rotor Modifications

Based on the reference geometry, 8 modifications were made to the compressor rotor, increasing or decreasing one of the key geometric parameters each time. A summary of all the cases analyzed is given in Table 2.

The main objective of the research presented in this article is to determine which key geometric parameters of the rotor have the most significant impact on the compression efficiency. The aim of the study is to maximize this efficiency by systematically modifying one independent variable at a time from the reference case and evaluating the performance using numerical tools. In addition to maximizing the efficiency for a given geometric modification, the potential of regulating the compressor over a rotational speed range from 400 RPM to 2400 RPM was also examined to identify the moment of a sudden efficiency drop at lower speeds due to reduced blade loading, flow instabilities caused by a low Reynolds number, an increased incidence angle, and possible flow separation.

The objective function in the considered case was to maximize the isentropic efficiency obtained from numerical simulations for each modified geometry of the compressor rotor. The optimization process focused on four independent variables, with each modified individually from the reference case, primarily to precisely isolate the influence of each variable on the efficiency. The independent variables selected for investigation were the following:

- Blade angle ξ (deg) : controls the flow turning and incidence angle;
- Blade solidity σ : defined as the ratio of the blade chord to the blade gap at the meanline;
- Blade thickness TH (%chord): determines the structural strength and aerodynamic shape;
- Hub-to-tip ratio HT : defines the radial distribution of the flow area.

Table 2 presents a description of all rotor geometry modifications along with the values of the modified independent variables relative to the base case.

Table 2. Redesign cases with rotor geometry modifications.

Independent Variable →	Blade Angle ξ (deg)	Blade Solidity at Meanline σ	Blade Thickness TH (%Chord)	Hub-to-Tip Ratio HT
case 1 (reference)	56.7	1.0	10	0.78
case 2	49.2	1.0	10	0.78
case 3	64.5	1.0	10	0.78
case 4	56.7	0.5	10	0.78
case 5	56.7	1.5	10	0.78
case 6	56.7	1.0	8	0.78
case 7	56.7	1.0	12	0.78
case 8	56.7	1.0	10	0.70
case 9	56.7	1.0	10	0.86

The first set of modifications concerned a change in the blade angle, which directly determines changes in the angle of attack. At low speeds, the angle of attack has a key impact on compressor efficiency. The second modification was to change the blade thickness, which directly affects the flow kinematics by determining the cross-sectional area and consequently the axial velocity. Additionally, the blade thickness influences profile losses, which significantly impact compressor performance. The third modification considered in this paper was blade solidity. In the high Reynolds number range, the optimum blade solidity has a value from about 0.8 to 1.2 [38] for flows with an inlet Mach number oscillating near 0.5. Solidity values were modified by changing the number of blades to achieve the desired value at the mean radius. The last modification was to examine the effect of the rotor size on compressor efficiency while keeping the same Reynolds number (defined by the chord

length, inlet velocity, and inlet density and viscosity under thermodynamic conditions). For the purpose of this modification, the compressor was redesigned by changing the ratio of hub-to-tip radius (HT) by 10% each compared with the reference case. All modifications were designed with the same relative kinematic parameters (related to the tip velocity), and the static pressure and velocity distributions at the inlet and outlet were recalculated using the free vortex radial equilibrium method, reproducing the design methodology used in [35].

To gain insight into the rotor's performance, a series of simulations was conducted, varying the rotor speed between 400 and 2400 RPM. This resulted in a Reynolds number range from 50,000 to 250,000, which is representative of the kinematics of the flow. A modification of the geometry (cases 8 and 9) was carried out with the objective of obtaining the same Reynolds number of 150,000. This allowed an assessment of the impact of the rotor size on the efficiency while maintaining a constant ratio of inertia forces to viscous flow forces.

2.4. Numerical Modeling

Computational Grid

A computational grid was produced for each of the modified geometries using Turbo-grid software [39]. The mesh type used was hexagonal grids comprising an O grid around the blades and an H grid within the flow channels. To improve the resolution in specific areas, namely the blade wall, the hub, and the tip, element densification was increased. This increased density in areas with high gradients provided greater resolutions, resulting in a more accurate representation of the flow conditions and loads in the analyzed rotors. The number of elements in each grid was in the range of 250,000–300,000. The grid was compacted in a manner which ensured that the dimensionless distance from the wall fell within the requisite range for the selected turbulence model. In the case of the model employed in this study (k- ω SST) [40], an accurate representation of the near-wall layer was achieved for y^+ values below 5. Figure 3 presents an overview of the grid for the reference case, accompanied by the y^+ distribution for the design case conducted within the velocity range corresponding to the highest rotational speeds. An analysis of the y^+ distribution revealed that the resulting value was consistently below 5 across the entire range of walls.

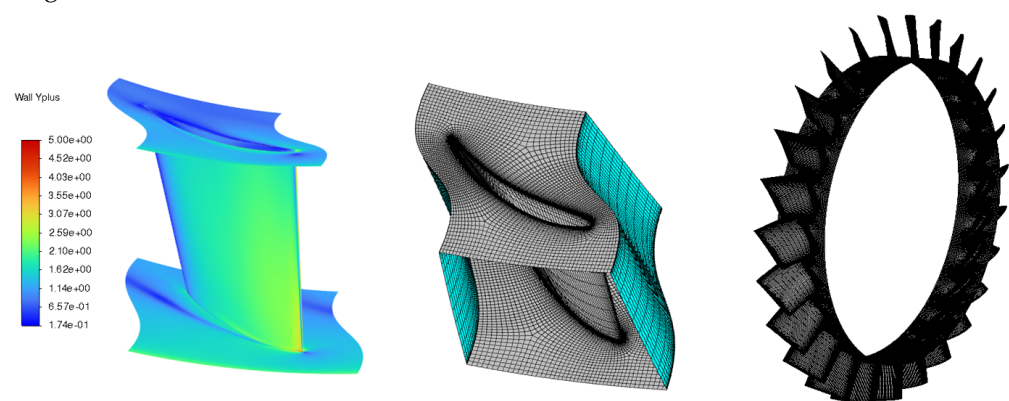


Figure 3. The y^+ verification and computational grid.

The grids were also evaluated for quality indicators, including skewness and orthogonality. The minimum orthogonal quality value was 0.4 for all cases analyzed, while the skewness was above 0.65. Additionally, when conducting the spatial discretization, a tip clearance value of 0.5% of the blade length was considered. This value was used in the reference case. Despite the fact that in actual systems, the tip clearance value is higher and

exceeds 1% of the blade length, it was decided to reduce the value to 0.5%. This approach was informed by the fact that in [35], the blades were created with this value to achieve a satisfactory level of agreement with the experimental results.

2.5. Grid Dependence Study

To make the numerical solution as accurate and stable as possible, the choice in grid size was preceded by a grid independence study. For the simulation, grids with 4 different values were created with a density factor of $r = 2$. Table 3 shows the characteristics of the meshes along with the obtained isentropic efficiency values calculated based on the area-weighted average values of the temperatures and stagnation pressures from the domain inlet and outlet. The simulation for the grid convergence study was conducted for a base case at a rotor speed of 1800 RPM. The discretization orders and algorithms for solving the system of conservative equations were consistent with those used in all simulations: a pressure-based coupled algorithm, a PRESTO scheme for the pressure correction equation, and QUICK for the convective terms. The absolute error was determined using Equation (2):

$$\epsilon = \left| \frac{\eta_{i+1} - \eta_i}{\eta_i} \right| \quad (2)$$

where η_i is the efficiency value for the simulation with the grid size described in Table 3. In the chart shown in Figure 4, it can be clearly seen that discrepancies in values due to grid size were minimal for the grids with more than 130,000 elements. The ϵ value for the first two grids was approximately 3.9%. For the subsequent ones, it was 0.18% and 0.07%. Since the absolute error value in the resolution range of grids larger than 150,000 was less than 1%, it was decided to use a grid size with approximately 250,000 elements, which represents a satisfactory balance between computational cost and solution accuracy.

Table 3. Summary of the sizes of the grids used for the grid independence study, the efficiency values obtained, and the absolute error of the values between the different grids.

i	Grid Size (-)	Average Element Size (mm)	Isentropic Efficiency η (%)	Absolute Error ϵ
1	60432	2.01	86.43	-
2	132678	1.54	83.1	3.9
3	241446	1.26	82.95	0.18
4	503489	0.99	82.89	0.07

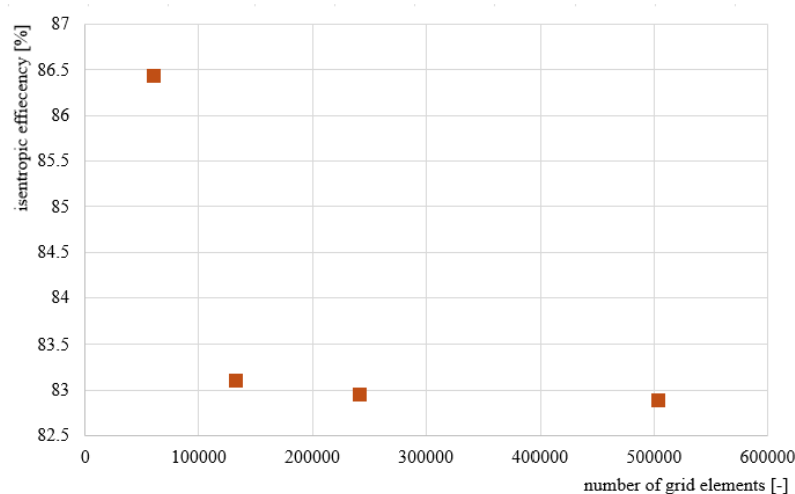


Figure 4. Value of isentropic efficiency of compression obtained for different grid sizes.

2.6. Turbulence Model

The $k-\omega$ SST model was selected as the turbulence model [40]. This hybrid approach combines the strengths of both the $k-\epsilon$ and $k-\omega$ models through the use of a blending function. It provides an accurate representation of the boundary layer while maintaining effective modeling of the free stream flow in the core region. Additionally, it includes a shear stress correction, which significantly enhances the modeling of flows where flow separation occurs, a phenomenon commonly observed in compressors, particularly near the suction side of the blade at the tip and hub regions. Recent validation studies conducted using this model [41–43] have shown that the $k-\omega$ SST model effectively captures the flow characteristics and performance of axial compressors. It is particularly effective in modeling flows in the stall region. Thus, the literature suggests that the $k-\omega$ SST turbulence model is the most appropriate choice for simulating complex flows in axial compressors, as it accurately represents the essential flow physics and delivers precise predictions of compressor performance.

Boundary Conditions, Discretization Methods, and Convergence Criteria

The boundary conditions employed in the numerical simulations were consistent across all cases under consideration. At the inlet, a pressure boundary condition was used, with the inlet value set to the atmospheric pressure. A pressure boundary condition was also applied at the outlet, with the static pressure value dependent on the rotor speed and the mass flow through the inter-blade flow channel. Since the simulation was conducted for a single blade, a periodic surface condition was implemented. The blade, hub, and tip walls were defined as no-slip walls. An illustration of the applied boundary conditions in relation to the rotor geometry is presented in Figure 5.

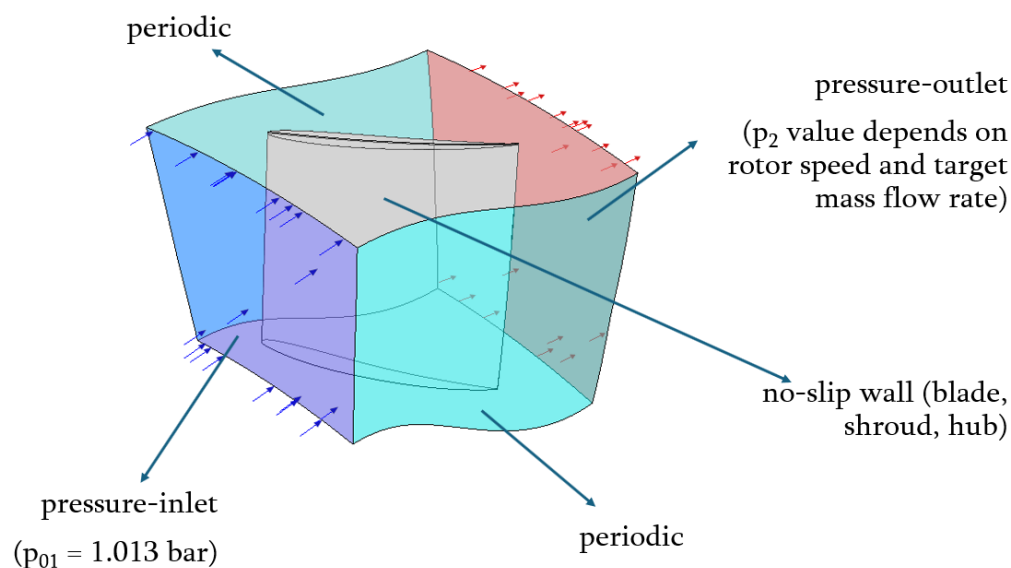


Figure 5. Overview of the boundary conditions used in the numerical simulation.

The flow field was obtained through the application of the Reynolds-averaged Navier–Stokes (RANS) equations. The pressure-based coupled method was employed for solving the system of equations using a pressure correction equation instead of the continuity equation. The equation was discretized using the Pressure Staggering Option (PRESTO) method. To solve the convection terms in the momentum transport and turbulence model equations, the Quadratic Upwind Interpolation for Convective Kinematics (QUICK) method, which is a hybrid of the central difference method and second-order upwind discretization, was used. This approach provides greater calculation stability. The calculations were considered

to have reached full convergence when the residuals were sufficiently low (below 10^{-4}) and when the mass flow rate values and upstream pressures at the inlet and outlet of the computational domain were observed to be stable.

2.7. Modified versus Classical Reynolds Number

For the purpose of research related to the influence of the diameter size on axial compressor rotor performance, it was decided to define a new parameter, that being a modified Reynolds number. With respect to its classical form, it differed in that its value was directly related to the mass flow rate and the diameter at the tip of the rotor. The modified version of the Reynolds number was transformed such that its value was directly proportional to the mass flow of gas supplied to the compressor (which directly influences the power requirement, particularly in the case of axial compressors, where the specific work per stage is relatively low in comparison with centrifugal machines) and the dimensions of the compressor rotor, determined by its diameter. Accordingly, the modified Reynolds number is expressed as follows in Equation (3). The classical Reynolds number is described by Equation (4):

$$Re_m = \frac{MFR}{D_t \cdot \mu} \quad (3)$$

$$Re = \frac{c_1 \cdot \rho \cdot \text{chord}}{\mu} \quad (4)$$

where c_1 is the velocity of the gas entering the rotor, ρ is the density at the rotor inlet, and μ is the dynamic viscosity. By utilizing the definitions of the mass flow rate, blade solidity, and assuming axial inflow with a constant chord length along the radius, a simple relationship between the considered parameters can be derived (Equation (5)). The full derivation is provided in Appendix A. The modified Reynolds number differs from its classical form by directly accounting for the hub-to-tip ratio HT , the blade solidity at the mean radius σ_m , and the number of blades N_{blades} :

$$\frac{Re_m}{Re} = \frac{(1 - HT)N_{blades}}{2 \cdot \sigma_m} \quad (5)$$

The modified Reynolds number differs from the classical definition in that the classical Reynolds number considers the ratio of inertial forces to viscous forces, with its value determining the intensification of the flow turbulence. The classical Reynolds number uses the blade chord length as the characteristic linear dimension but does not directly account for rotor geometry or the pressure ratio, which determines the aerodynamic loading of the blade. The modified Reynolds number, on the other hand, features a formulation which directly incorporates the mass flow rate and rotor size. It can be applied in cases where two scenarios theoretically have the same Reynolds number, yet observable differences in isentropic efficiency arise due to the occurrence of secondary flow phenomena in turbulent flow. This particular scenario was chosen for testing in the research described in this publication. The modified Reynolds number, in addition to accounting for effects related to turbulent flows, also considers geometric modifications to the rotor, making it a complementary criterion for maintaining high efficiency in cases where the classical Reynolds number is an insufficient indicator.

3. Results and Discussion

In order to assess the pressure rise across the designed compressor rotor, dimensionless parameters defining the change in the total and static pressure in relation to the tip velocity-dependent dynamic pressure and stagnation pressure at the inlet to the domain were

employed. The rise factor of the total pressure value was as defined by Equation (6). The static pressure rise factor was calculated using the following formula (Equation (7)):

$$\text{TPRC} = \frac{p_{02} - p_{01}}{\frac{1}{2}\rho U_t^2} \quad (6)$$

$$\text{SPRC} = \frac{p_2 - p_1}{\frac{1}{2}\rho U_t^2} \quad (7)$$

The adiabatic efficiency (Equation (8)) of the rotor was determined from an empirical formula using the predicted value of the lift coefficient, which was determined from the results of experimental cascade studies. This value was averaged over the flow parameters, including the resulting relative inflow angles (β_1), angle of attack (α), and blade turn angle (θ), for five control cross-sections along the rotor radius (hub, inboard, pitch, outboard, and tip) [44]:

$$\eta_{ad} = 1 - \frac{1}{(LD + \tan \beta_m) \tan \beta_1 \cos^2 \beta_m} \quad (8)$$

$$\beta_m = \tan^{-1} \frac{\tan \beta_1 + \tan \beta_2}{2} \quad (9)$$

Figure 6 illustrates the simulation results for the reference case compared with the experimental values, including the associated error bars. The results for the adiabatic efficiency exhibited a discrepancy of approximately 2% with respect to the experimental data. However, the discrepancies between the measured TPRC and SPRC values were deemed to be within an acceptable range. It can thus be concluded that the numerical scheme employed to obtain the flow fields accurately determined the values of the flow variables and could be utilized to analyze the flow field in modified geometric cases of the reference rotor. The values obtained using this efficiency definition were smaller than those obtained using the empirical formula. The latter assumes the value of the lift-to-drag ratio LD , which can be obtained in a full rotor system with a stator, thereby improving the stability of the flow field. Additionally, the empirical formula is dedicated to rotors with a higher Reynolds number than the range considered in this paper (above 500,000). It should be noted that the efficiencies obtained using this approach were higher than the actual ones.

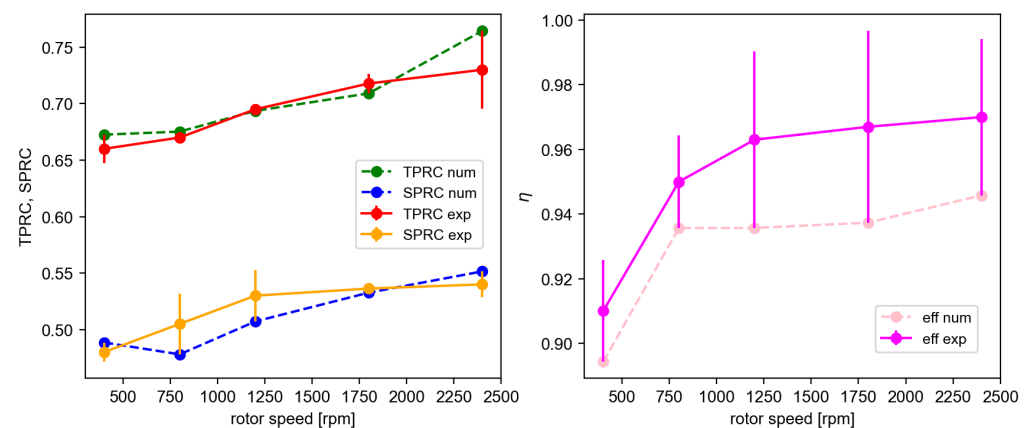


Figure 6. Comparison of numerical and experimental data for the reference case.

Given the empirical nature of the adiabatic efficiency formula, the results obtained are not reliable for determining actual efficiencies within the range of Reynolds numbers considered, as the parameters used in the formula were based on approximate values for the entire rotor cascade. Consequently, in the remainder of this article, the method

for determining the rotor efficiency is modified, using a direct definition of the isentropic compression efficiency to obtain the efficiency derived directly from the kinematics obtained from the simulated flow (Equation (10)):

$$\eta = \frac{l_{1-2s}}{l_{1-2}} = \frac{c_p T_{01}}{l_{1-2}} \left[\left(\text{TPRC} \cdot \frac{\rho U_t^2}{2p_{01}} + 1 \right) - 1 \right] \quad (10)$$

3.1. Comparison of the Compressor Rotor Efficiency Definitions Used

Table 4 presents a comparison of the two efficiencies: those obtained using the empirical formula (Equation (8)) and those derived from the classical definition of isentropic efficiency (Equation (10)) for the reference case.

Table 4. Comparison of efficiency values defined by the empirical formula [35] and the classical isentropic definition.

ω (RPM)	η_{ad} (%)	η (%)
400	89.43	73.73
800	93.57	78.07
1200	93.57	80.16
1800	93.73	82.31
2400	94.58	84.43

The values obtained using the empirical formula (Equation (8)) were approximately 10–18% higher than those derived from the classical definition (Equation (10)). These differences may stem from several key factors. The first is that one of the parameters assumed in the efficiency definition is the lift-to-drag ratio LD , which is determined based on the rotor's geometric parameters and predicts the value for the entire stage. This value is generally higher than that obtained for the rotor alone, as the presence of the stator stabilizes the flow field and reduces flow losses. The second key factor is that the tabulated data available in [44] were based on experiments conducted at higher Reynolds numbers than those considered in the experiment reported in [35]. Compressors operating at higher Reynolds numbers exhibit greater stability in the flow field and higher blade loading, which translates into higher efficiency values. In the experimental data, the same coefficients were used, but there were insufficient data to evaluate the efficiency according to the classical definition due to the lack of temperature measurements downstream of the rotor. Theoretically, it is possible to reconstruct the experimental value retrospectively by determining the relative angle changes from the efficiency definition and using them to calculate temperature changes through the definitions of stagnation enthalpy and velocity triangles for a two-dimensional cascade. However, the authors argue that applying these two simplifications does not capture the full flow field and introduces another series of approximations, leading to an even more underestimated isentropic efficiency definition. For this reason, the authors decided to use the empirical formula (Equation (8)) for numerical scheme validation. Despite potentially overestimating the efficiency values through the tabulated LD coefficient, the formula effectively represents the flow kinematics at equivalent efficiency values. This directly influences the accurate representation of the pressure field and, consequently, the resulting work and efficiency, particularly in the case of incompressible flows.

3.2. Influence of Blade Angle

Figure 7 illustrates the correlation between the resulting pressure increase coefficients and rotor speed, as well as the dependence between the isentropic compression efficiency and the Reynolds number. The incidence and deflection angles of the flow are influenced

by the blade angles, which in turn affect the energy transfer from the rotor to the fluid. The optimal blade angle minimizes flow separation and reduces aerodynamic losses, thereby enhancing the efficiency of the compressor. From the graph, it can be observed that the rotor achieved higher efficiency values for higher blade angles within the range of 74–84%. Furthermore, it can be seen that increasing the blade angle did not result in a significant improvement in compression efficiency. However, it is noteworthy that the highest values for the static pressure increase were obtained for the design's blade angle. An increase in the angle of attack resulted in a reduction in the static pressure increase, which was directly reflected in the flow kinematics. The axial velocity values obtained were higher, which generally improved the rotor performance. However, this also increased the losses associated with a higher turbulence intensity, which in turn contributed to the potential occurrence of secondary phenomena related to secondary flows and an increasing boundary layer. These two factors are in equilibrium with one another, resulting in comparable efficiencies for the optimum and increased blade angles. A reduction in the blade angle to 49.2 degrees resulted in a notable decline in compression efficiency, particularly within the lower Reynolds number range under consideration. The elevated losses are attributable to localized flow separation, which gives rise to augmented flow losses and a concomitant reduction in efficiency.

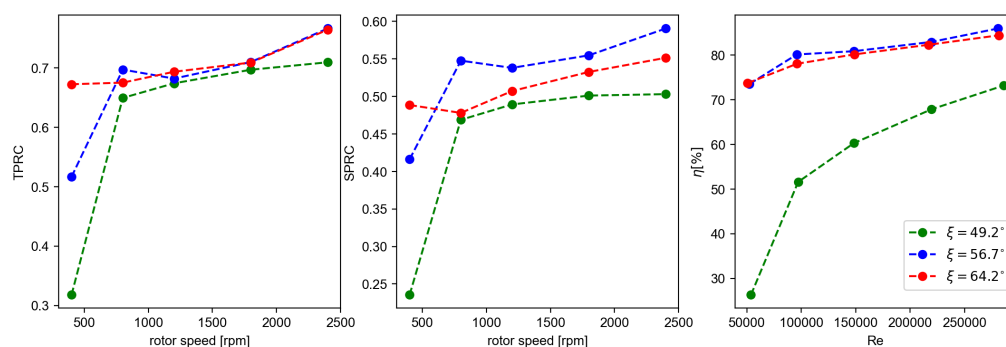


Figure 7. The effect of the blade angle on the pressure rise coefficients and efficiency.

In all cases analyzed, a trend can be observed where the efficiency declined at Reynolds numbers less than 100,000. At a rotational speed of 400 RPM, the tip velocity was approximately 15 m/s. The low velocity range gave rise to a number of phenomena resulting in a reduction in rotor efficiency. At lower speeds, the resulting angle of attack was suboptimal, resulting in improper attachment of the fluid to the blade surface. This consequently increased the risk of boundary layer separation and the formation of turbulence structures, which in turn increased energy loss. A reduction in the flow angle resulted in a significant decline in efficiency, reaching a value of 28%. A detailed examination of the flow field depicted in Figure 8 revealed the precise location of the area of the tip leakage vortex. In the case of larger blade angles, separation was not observed at low speeds. However, due to the low kinetic energy, the flow stability was underestimated, and the pressure increase values were significantly lower. This also led to a decrease in rotor efficiency of approximately 5%.

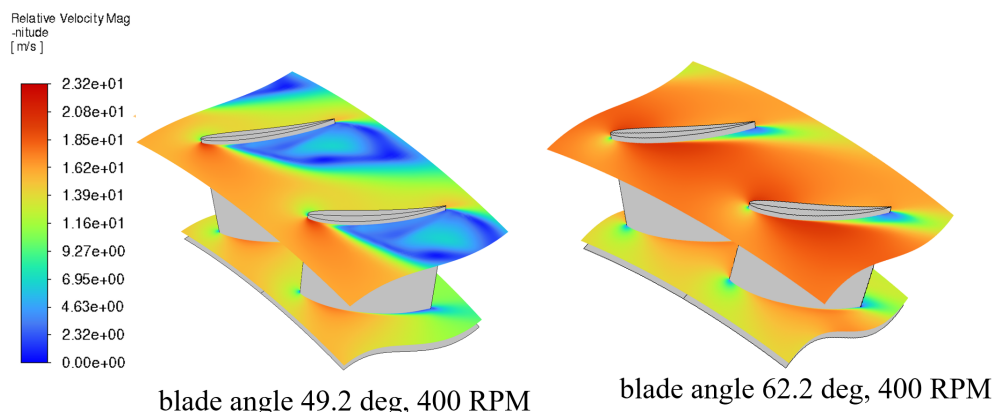


Figure 8. Relative velocity distribution near the tip. For the lower blade angle, separation of flow occurred.

3.3. Influence of Blade Thickness

Figure 9 illustrates the analyzed parameters which were considered with varying blade thicknesses. An increase in blade thickness results in a larger contact area with the flow, which in turn leads to an increase in profile drag. This results in increased energy losses, as a proportion of the rotor power is consumed in overcoming the drag generated by the thicker profile. This phenomenon is illustrated in the graphs, which demonstrate that a thicker blade exhibits markedly lower pressure increase and efficiency values. An increase in blade thickness may result in elevated shear stresses at the blade surface, which could contribute to augmented viscous losses. Furthermore, an increased profile thickness modifies the velocity distribution at the blade walls, which may intensify the losses associated with the boundary layer. The highest efficiency values were obtained for the thinner blade thicknesses, as thinner blades serve to minimize these phenomena. It is important to note that manufacturing smaller blades is a technically challenging process, and they possess reduced mechanical strength, which increases their vulnerability to vibration, particularly at higher speeds. Furthermore, they exhibit reduced resistance to damage and erosion. It is thus essential that the design process strikes a balance between achieving adequate mechanical strength and minimizing the impact of secondary phenomena on the flow.

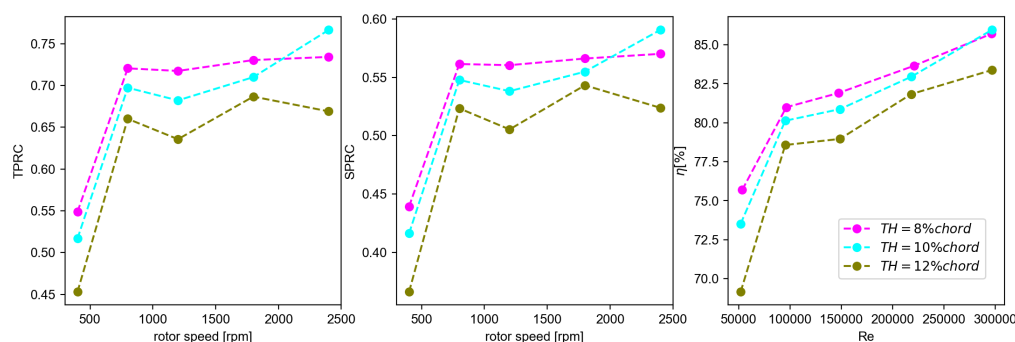


Figure 9. The effect of the blade thickness on the pressure rise coefficients and efficiency.

3.4. Influence of Blade Solidity

A review of the data presented in Figures 10 and 11 revealed that modifying the blade solidity from the optimal value recommended in [38] (1.0) resulted in a reduction in efficiency across both cases. However, the decline in efficiency was more pronounced in the rotor with the higher solidity, with an average decrease of 10% observed across the range of rotor speeds under consideration. An increase in the Reynolds number was associated with an enhancement in efficiency. At the lowest flow speeds, the compression efficiency

was observed to decrease to a value of 65%. In theory, an increase in blade solidity should improve the efficiency due to a reduction in the intensity of secondary phenomena, higher flow stability, and resistance to blade overloading. However, all indices were analyzed within the higher Reynolds range. In the lower velocity range, increased blade solidity resulted in higher aerodynamic drag losses, which were directly related to the profile shape. For the NACA65 profile, the optimal solidity value, as determined in [35], is 1.0. This value also represents the optimal solidity for low Reynolds numbers.

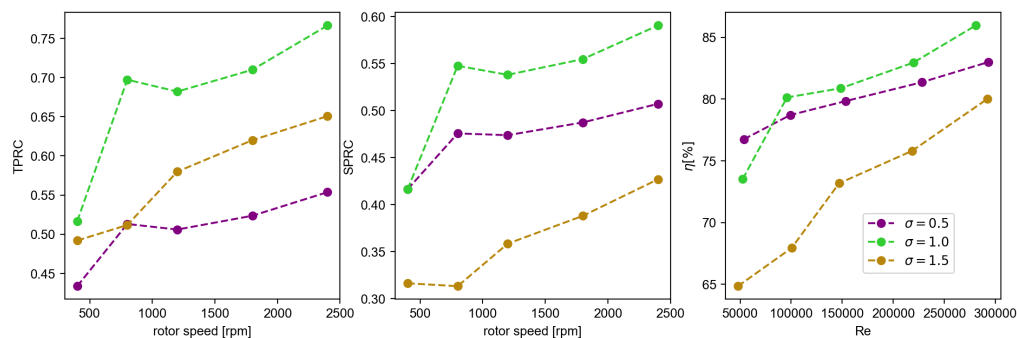


Figure 10. The effect of the blade solidity on the pressure rise coefficients and efficiency.

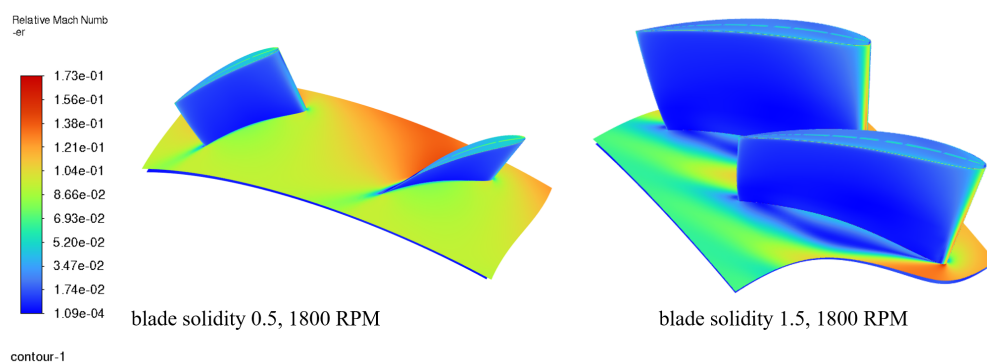


Figure 11. Relative Mach number distribution. Hub corner separation for the modified case with a solidity of 1.5 can be observed.

3.5. Influence of Rotor Size

Given the crucial role of size in HVAC systems, the dimensions of the rotor significantly impact the ultimate dimensions of the drive unit in such systems. While a direct approach would involve geometrically scaling the compressor rotor, this study adopted a more indirect approach. In the context of an air-conditioning system designed in collaboration with industries, the client's specifications, including those concerning rotor size, guided the development of a high-efficiency axial compressor whose operating point aligned with kinematics which imposed a Reynolds number of approximately 150,000. As previously discussed in relation to compressor efficiency, an analysis of the graphs for different geometrical parameters revealed that within this range, the efficiency of the compression process reached approximately 80% for an optimal choice of parameters. It was therefore decided to implement the final modification by adjusting the rotor diameter (through modification of the hub-to-tip ratio) while maintaining the Reynolds number. Table 5 presents a comparison of the resulting rotor geometry and compressor mass flow rates when the hub-to-tip ratio was modified by approximately 10% while maintaining the same mid-radius kinematic parameters.

Table 5. Rotor size modification data.

HT	Re	Re _m	TPRC	SPRC	MFR (kg/s)	D _t (m)
0.70	153,522	548,228	0.67	0.84	6.97	0.74
0.78	148,674	365,619	0.68	0.53	4.45	0.71
0.86	149,745	284,207	0.69	0.56	3.31	0.68

Figure 12 illustrates the dependence between the analyzed flow variables and the Reynolds number and modified Reynolds number for all cases under consideration. A reduction in the rotor diameter (and an increase in the hub-to-tip ratio) had a direct effect on the modified Reynolds number. It can be observed that the higher the value, the larger the efficiency achieved. The modified Reynolds number is dependent on both the mass flow rate and the rotor diameter. Therefore, by comparing it as an argument of a function of efficiency, it was possible to observe a much clearer effect from the rotor size on the efficiency than with the classical definition of the Reynolds number. It is evident that an increase in diameter resulted in enhanced efficiency, which was also directly correlated with the increased flow area. This allowed better compression with lower pressure losses, thereby improving the efficiency. In the high Reynolds number range, a reduction in the hub-to-tip ratio resulted in a decline in efficiency, attributable to the emergence of secondary phenomena within the flow. Nevertheless, in the lower velocity range, the intensity of secondary phenomena was considerably diminished, thereby enabling longer blades to achieve higher efficiencies. In the low Reynolds range (and thus a lower velocity range), the separation of the boundary layer occurring at the hub (as illustrated in Figure 13) exerted a considerable influence on the efficiency. The smaller the span, the more pronounced this effect was. A higher hub-to-tip ratio implies a more significant role for the area surrounding the hub, where the flow is frequently more turbulent and subject to larger viscous losses.

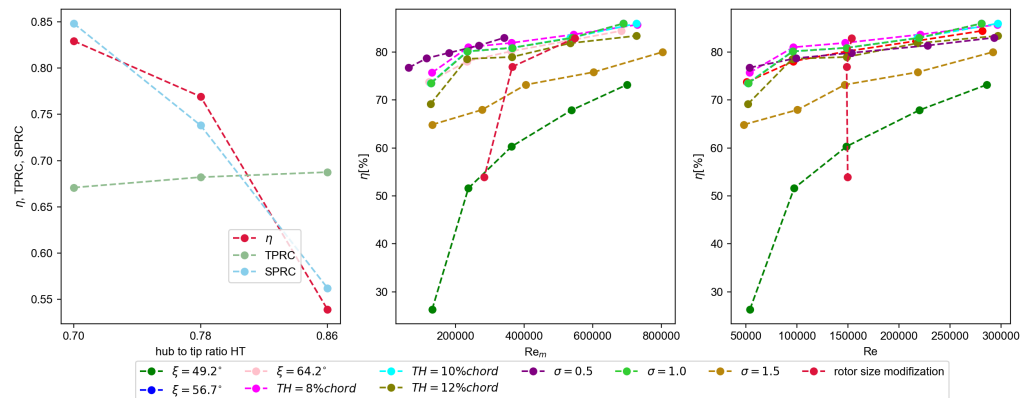


Figure 12. The effect of the rotor size on the pressure rise coefficients and efficiency (left chart) and efficiency in terms of Re and modified Re numbers.

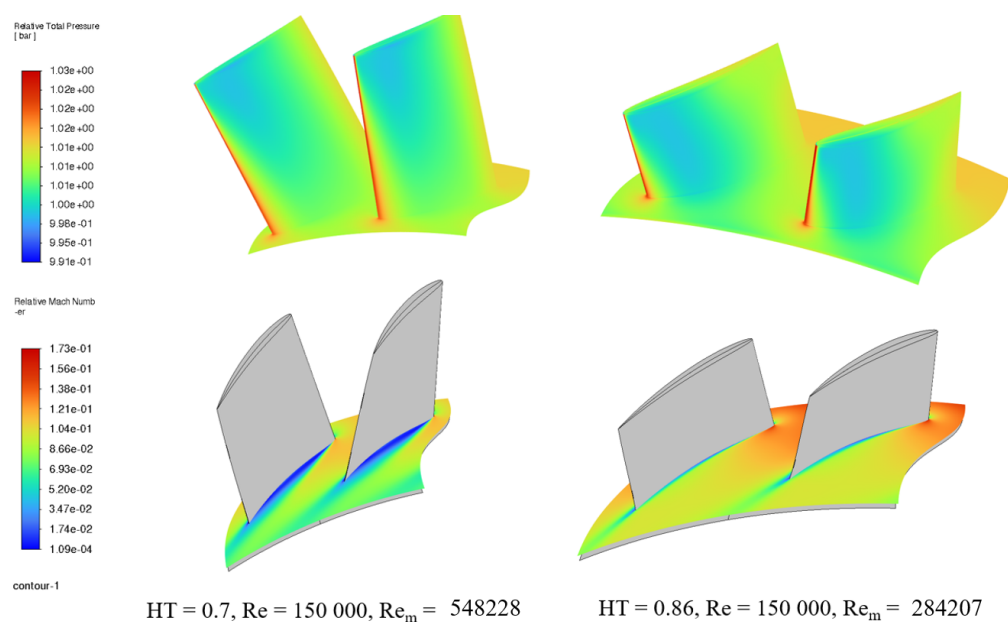


Figure 13. Relative total pressure and relative velocity distribution near the hub.

4. Discussion

The studies conducted within the scope of this publication aimed to evaluate the potential of using axial compressors in low-power systems. The research included an in-depth numerical analysis (based on a validated numerical scheme) of various geometric configurations of the compressor rotor, focusing on the achieved isentropic efficiency across different rotational speed ranges of the rotor. Regardless of the geometric modifications introduced to the rotor, the isentropic efficiency of compression reached maximum values at the highest rotational speeds considered, corresponding to higher Reynolds number ranges (above 200,000). A decrease in efficiency was observed at rotational speeds below 800 RPM, corresponding to Reynolds numbers lower than 150,000. The compression process efficiency values oscillated between 80 and 85% in the higher Reynolds number range. Efficiency drops in all analyzed cases resulted from flow instability due to reduced velocities. Flow field analysis indicated that the primary flow phenomena responsible for reducing efficiency were boundary layer separation near the hub and the tip of the rotor. Table 6 provides a summary of the maximum and minimum efficiency values for the highest and lowest rotational speeds of the compressor rotor.

Table 6. Summary of the maximum and minimum efficiencies obtained for the considered geometric modifications of the rotor.

Case ID	Independent Variable Changed	η_{max} (%)	η_{min} (%)	$\eta_{max} - \eta_{min}$ (%)
case 1	reference case	85.95	73.52	12.43
case 2	blade angle decreased -7.5 deg	73.19	26.30	46.89
case 3	blade angle decreased $+7.5$ deg	84.43	73.73	10.71
case 4	blade solidity -0.5	82.99	76.75	6.24
case 5	blade solidity $+0.5$	80.00	64.85	15.15
case 6	blade thickness increased -2% chord	85.71	75.70	10.01
case 7	blade thickness decreased $+2\%$ chord	83.38	69.16	14.23
caseID	independent variable changed	η for Re = 150,000		
case 8	HT = 0.70	82.92		
case 9	HT = 0.86	53.92		

The greatest improvement in efficiency was achieved in two cases: for a blade angle increased by 7.5 degrees relative to the reference case and for a blade chord thickness reduced by 2% of the chord length. In both cases, the efficiency reached approximately 86%. While the reduced rotor size may pose technological challenges in achieving a thinner blade thickness, increasing the blade angle appears to be a promising approach for achieving a more efficient rotor blade design. The lowest efficiency across all rotational speeds was observed when the blade angle was reduced to approximately 50 degrees. At the highest rotational speed considered, the efficiency was roughly 73%, while a significant drop to 26% was observed as the rotor speed decreased to 400 RPM. This substantial decline was caused by severe flow separation near the blade tip due to pronounced flow destabilization. Reduced compressor performance in terms of efficiency (80% at 2400 RPM and 65% at 400 RPM) was observed when the blade solidity was increased to a value of 1.5. This modification resulted in a higher contribution of the boundary layer to the flow and the occurrence of hub corner separation. This is an interesting observation because in compressors operating at higher loads, the trend is usually the opposite; for aspect ratios greater than 1.0, efficiency typically increases. However, in high-speed compressors, the relative thickness of the boundary layer in the flow is significantly smaller.

Another aspect considered in the studies was the analysis of how rotor speed regulation affects compressor efficiency. By examining the differences between the maximum and minimum efficiency values achieved within the considered range of rotational speeds, it can be observed that a rotor with a reduced blade solidity of 0.5 exhibited the most stable operating range, with an efficiency drop due to a rotational speed reduction of approximately 6%. Efficiency drops of about 10% were observed for the two cases achieving the highest efficiencies. Given that these efficiency drops are minor compared with the performance characteristics of centrifugal and scroll compressors, it can be concluded that axial compressors have significant potential for applications requiring a wide range of compressed gas distribution, which can be achieved through rotor speed regulation (while maintaining the same relative total pressure ratio increase).

The introduction of a new parameter, the modified Reynolds number, did not significantly change the efficiency curves when compared to the classical definition in most cases. The modified Reynolds number differs from the classical definition by directly accounting for the compressor size, which determines the mass flow rate while preserving the same flow kinematics at the rotor. However, it demonstrated significant potential in comparative analyses of compressors operating within a similar range of classical Reynolds numbers (in the case of this study, approximately 150,000). By altering the rotor size through changes in the hub-to-tip ratio, different efficiency values were achieved, even while maintaining the same ratio of viscous to inertial forces in the flow. When comparing efficiency drops as a function of the modified Reynolds number, distinct values were observed. For a hub ratio of 0.7 (corresponding to a Reynolds number of approximately 153,000 and a modified Reynolds number of 550,000), the rotor efficiency was highest, being approximately 83%. At the highest hub-to-tip ratio (HT) of 0.86 ($Re = 149,700$ and $Re_m = 285,000$), the efficiency dropped to 54%. Thus, it can be concluded that increasing the modified Reynolds number improves efficiency, even though the classical definition suggests that the efficiency should remain constant. In specific cases, the modified Reynolds number may prove to be a promising parameter in the design process, particularly when the classical Reynolds number is insufficient for evaluating the predicted rotor efficiency of an axial compressor.

5. Conclusions

Axial compressors are highly efficient for large-scale applications. However, their use in small-scale HVAC and combustion systems is limited due to factors such as their

high cost, mechanical complexity, and low efficiency at reduced flow rates. Nonetheless, advancements in miniaturization and energy efficiency could enable the integration of axial compressors into these systems, particularly for specialized applications requiring compact designs and precise flow control.

This study aimed to explore the potential use of axial compressors in low-power systems, where the operational range of the rotor's Reynolds numbers was limited to below 250,000. The maximum isentropic efficiency was achieved for geometric configurations with blade angles increased by 7.5 degrees compared with the reference case (up to 64.5 degrees) and for rotors with a blade thickness reduced by 2% of the chord length relative to the reference case. The maximum efficiency values, which were approximately 86% for both configurations, were attained at Reynolds numbers near 250,000. These configurations also demonstrated significant potential for systems requiring a wide range of speed control, with a maximum efficiency drop of about 10%. The achieved efficiency values are relatively low compared with those typically attainable for axial compressors. This is attributed to the simulations being conducted on a potential first-stage compressor, which inherently has the lowest efficiency, and the absence of a stator, which would otherwise enhance flow stability and improve efficiency. The most stable operation range, with an efficiency drop of about 6%, was observed for a reduced blade solidity ($\sigma = 0.5$). The most pronounced negative impact on efficiency (a drop of approximately 10–45%, depending on the rotor speed) occurred when the blade angle was reduced to 50 degrees and the aspect ratio was increased to $\sigma = 1.5$, with a maximum efficiency drop of 15%. The largest efficiency reductions were observed at the lowest rotational speeds of 400 RPM, where low-speed conditions significantly reduced flow stability, leading to pronounced tip vortex formation and hub corner separation. Significant discrepancies in cases with reduced efficiency were primarily linked to variations in static pressure, which directly influenced flow kinematics. While reducing the blade thickness can enhance rotor efficiency, it may compromise the durability. For the blade geometry under consideration, the optimal solidity value was approximately one. Deviations from this value—either increasing or decreasing the solidity—resulted in reduced compression process efficiency.

The modified Reynolds number may prove to be a useful parameter in compressor design, as it is directly determined by the required mass flow rate and diameter size, especially in cases where different geometric variants of a rotor with similar flow kinematics operate within the same range of classical Reynolds numbers (defined in terms of inlet velocity, density, and chord length).

Further research should be conducted to evaluate the modified Reynolds number through a more rigorous approach, specifically by directly scaling the compressor rotor. Additionally, the efficiency of the compressor rotor in interaction with the stator and in a multistage variant should be assessed.

Author Contributions: Conceptualization, N.K.; methodology, N.K.; software, N.K.; validation, N.K.; formal analysis, N.K.; investigation, N.K. and A.F.; writing—original draft preparation, N.K. and A.F.; writing—review and editing, N.K. and K.W.; visualization, N.K. and K.W.; supervision, A.F. All authors have read and agreed to the published version of the manuscript.

Funding: This research was funded by the European Regional Development Fund under the Intelligent Development Programme grant number POIR.01.01.01-00-0223/21.

Acknowledgments: Grant No. POIR.01.01.01-00-0223/21, entitled 'Development and demonstration of an air cooling and heating device based on a flow machine operating without harmful working agents', was co-financed by the European Union through the European Regional Development Fund

under the Intelligent Development Programme. The project was implemented under a competition of the National Centre for Research and Development: Fast Track.

Data Availability Statement: The original contributions presented in this study are included in the article. Further inquiries can be directed to the corresponding author(s).

Conflicts of Interest: The authors declare no conflicts of interest.

Nomenclature

Symbols:

CL	Lift coefficient (-)
c_p	Specific heat (J/(kg K))
D_t	Compressor rotor tip diameter (m)
l_{1-2}	Specific work (J/kg)
l_{1-2s}	Isentropic specific work (J/kg)
n	Rotor speed (RPM)
N_{blades}	Number of rotor blades
p_0	Total pressure (bar)
p	Static pressure (bar)
Re	Reynolds number (-)
Re_m	Modified Reynolds number (-)
T_0	Total temperature
TH	Blade thickness (m)
U_t	Tip velocity (m/s)
w	Relative velocity (m/s)
y^+	Dimensionless wall distance (-)

Greek symbols:

α	Angle of attack (deg)
β	Relative angle (deg)
η	Efficiency (-)
θ	Air turning angle (deg)
μ	Dynamic viscosity (Pa·s)
ξ	Blade angle (deg)
ρ	Density (kg/m ³)
σ	Blade solidity (-)

Abbreviations

The following abbreviations are used in this manuscript:

COP	Coefficient Of power
CFD	Computational fluid dynamics
GCI	Grid convergence index
HVAC	Heating, ventilation, and air conditioning
HT	Hub-to-tip ratio
LD	Lift-to-drag ratio
MFR	Mass flow rate
MUSCLE	Monotonic Upstream-Centered Scheme for Conservation Laws
NACA	National Advisory Committee for Aeronautics
RANS	Reynolds-averaged Navier–Stokes
SPRC	Static pressure rise ratio
TPRC	Total pressure rise ratio
QUICK	Quadratic Upstream Interpolation for Convective Kinematics

Appendix A

This appendix contains a detailed derivation of the relationship between the classical Reynolds number and its modified form, proposed in this article as an alternative version which can be used for evaluating compressor efficiency. The classical Reynolds number is defined as follows:

$$Re = \frac{c_1 \cdot \rho \cdot \text{chord}}{\mu} \quad (\text{A1})$$

where c_1 is the inlet gas's absolute velocity, ρ is the inlet gas's density, and μ is the gas's dynamic viscosity. The modified Reynolds number is defined as follows:

$$Re_m = \frac{\text{MFR}}{D_t \cdot \mu} \quad (\text{A2})$$

The mass flow rate entering the compressor rotor is expressed by

$$\text{MFR} = c_1 \cdot \cos \alpha_1 \cdot \rho \cdot A_1 \quad (\text{A3})$$

where α_1 is the absolute inlet flow angle and A_1 is defined as the cross-sectional flow area at the inlet to the rotor. For the assumption of axial flow and defining the inlet area to the rotor A_1 through the diameter at the rotor tip and the hub-to-tip ratio HT , we have

$$\text{MFR} = c_1 \cdot \rho \cdot \frac{1}{4} \pi D_t^2 (1 - HT^2) \quad (\text{A4})$$

Combining Equation (A2) with Equation (A4) gives

$$Re_m = \frac{c_1 \cdot \rho \cdot \pi D_t^2 (1 - HT^2)}{4 \cdot D_t \cdot \mu} \quad (\text{A5})$$

The definition of the modified Reynolds number can be transformed to incorporate the definition of the classical Reynolds number:

$$Re_m = \frac{c_1 \cdot \rho \cdot \pi D_t^2 (1 - HT^2)}{4 \cdot D_t \cdot \mu} \cdot \frac{\text{chord}}{\text{chord}} = \frac{c_1 \cdot \rho \cdot \text{chord}}{\mu} \cdot \frac{\pi D_t^2 (1 - HT^2)}{4 \cdot D_t \cdot \text{chord}} = Re \cdot K \quad (\text{A6})$$

Assuming that the studies on the rotor geometry's impact do not modify the diameter, chord length, or hub-to-tip ratio, it can be assumed that the modified Reynolds number changes proportionally with the classical one. This proportionality is nonlinear when modifications to these parameters occur. The term K is now defined as a dependency solely based on the rotor geometry:

$$K = \frac{\pi D_t^2 (1 - HT^2)}{4 \cdot D_t \cdot \text{chord}} \quad (\text{A7})$$

The above expression can be transformed to incorporate the chord length and the blade's spanwise extension at the mean radius using the following auxiliary relationships:

- The blade solidity at the tip is expressed by

$$\sigma_t = \frac{\text{chord}}{\text{gap}_t} = \frac{\text{chord}}{\frac{\pi D_t}{N_{\text{blades}}}} = \frac{\text{chord} \cdot N_{\text{blades}}}{\pi D_t} \quad (\text{A8})$$

- The mean rotor diameter can be defined using the hub-to-tip ratio and the tip diameter:

$$D_m = \frac{D_t + D_h}{2} = \frac{D_t(1 + HT)}{2} \rightarrow D_t = \frac{2D_t}{1 + HT} \quad (\text{A9})$$

- By combining Equation (A8) with Equation (A9), it is possible to derive a relationship between the blade solidity at the tip and the blade solidity at the mean radius σ_m :

$$\sigma_t = \frac{\text{chord} \cdot N_{\text{blades}}(1 + HT)}{2\pi D_m} = \sigma_m \cdot \frac{1}{2}(1 + HT) \quad (\text{A10})$$

Equation (A7) can be modified to include the variable σ_t :

$$K = \frac{\pi D_t}{\text{chord} \cdot N_{\text{blades}}} \cdot \frac{N_{\text{blades}} \cdot (1 - HT^2)}{4} = \frac{1}{\sigma_t} \cdot \frac{N_{\text{blades}} \cdot (1 - HT^2)}{4} \quad (\text{A11})$$

By combining Equation (A7) with Equation (A10), we have

$$K = \frac{1}{\sigma_m} \cdot \frac{2N_{\text{blades}}(1 - HT)(1 + HT)}{4(1 + HT)} = \frac{(1 - HT)N_{\text{blades}}}{2\sigma_m} \quad (\text{A12})$$

At the same time, the constant K represents the ratio between the modified and classical Reynolds numbers:

$$\frac{Re_m}{Re} = K = \frac{(1 - HT)N_{\text{blades}}}{2\sigma_m} \quad (\text{A13})$$

References

1. Llopis, R.; Nebot-Andrés, L.; Sánchez, D.; Catalán-Gil, J.; Cabello, R. Subcooling Methods for CO₂ Refrigeration Cycles: A Review. *Int. J. Refrig.* **2018**, *93*, 85–107. [[CrossRef](#)]
2. Pérez-Lombard L.; Ortiz, J.; Pout, C.T. A Review on Buildings Energy Consumption Information. *Energy Build* **2008**, *40*, 394–398. [[CrossRef](#)]
3. Sukri, M.F.; Salim, M.A.; Mohd Rosli, M.A.; Azraai, S.B.; Mat Dan, R. An Analytical Investigation of Overall Thermal Transfer Value on Commercial Building in Malaysia. *Int. Rev. Mech. Eng.* **2012**, *6*, 1050–1056.
4. Sumeru, K.; Pramudantoro, T.P.; Setyawan, A.; Muliawan, R.; Tohir, T.; bin Sukri, M.F. Effect of Compressor-Discharge-Cooler Heat-Exchanger Length Using Condensate Water on the Performance of a Split-Type Air Conditioner Using R32 as Working Fluid. *Energies* **2022**, *15*, 8024. [[CrossRef](#)]
5. Kim, J.; Song, D.; Kim, S.; Park, S.; Choi, Y.; Lim, H. Energy-Saving Potential of Extending Temperature Set-Points in a VRF Air-Conditioned Building. *Energies* **2020**, *13*, 2160. [[CrossRef](#)]
6. Qureshi, T.Q.; Tassou, S.A. Variable-Speed Capacity Control in Refrigeration Systems. *Appl. Therm. Eng.* **1996**, *16*, 103–113. [[CrossRef](#)]
7. Mei, J.; Xia, X. Energy-efficient predictive control of indoor thermal comfort and air quality in a direct expansion air conditioning system. *Appl. Energy* **2017**, *195*, 439–452. [[CrossRef](#)]
8. Kwon, L.; Hwang, Y.; Radermacher, R.; Kim, B. Field Performance Measurements of a VRF System with Sub-Cooler in Educational Offices for the Cooling Season. *Energy Build* **2012**, *49*, 300–305. [[CrossRef](#)]
9. Bilir, N.; Ersoy, H.K. Performance Improvement of the Vapour Compression Refrigeration Cycle by a Two-Phase Constant Area Ejector. *Int. J. Energy Res.* **2009**, *33*, 469–480. [[CrossRef](#)]
10. Arsana, M.E.; Kusuma, I.G.B.W.; Sucipta, M.; Suamir, I.N. Thermodynamic Analysis of Two-Phase Ejector as Expansion Device with Dual Evaporator Temperatures on Split Type Air Conditioning Systems. *IOP Conf. Ser. Mater. Sci. Eng.* **2019**, *494*, 12034. [[CrossRef](#)]
11. Zilio, C.; Brignoli, R.; Kaemmer, N.; Bella, B. Energy efficiency of a reversible refrigeration unit using R410A or R32. *Sci. Technol. Built Environ.* **2015**, *21*, 502–504. [[CrossRef](#)]
12. Barve, A.; Cremaschi, L. Drop-in performance of low GWP refrigerants in a heat pump system for residential. In Proceedings of the International Refrigeration and Air Conditioning Conference at Purdu, West Lafayette, IN, USA, 16–19 July 2012; p. 2197.
13. Yang, M.; Wang, B.; Li, X.; Shi, W.; Zhang, L. Evaluation of two-phase suction, liquid injection and two-phase injection for decreasing the discharge temperature of the R32 scroll compressor. *Int. J. Refrig.* **2015**, *59*, 269–280. [[CrossRef](#)]
14. Shuxue, X.; Guoyuan, M.; Qi, L.; Zhongliang, L. Experiment study of an enhanced vapor injection refrigeration/heat pump system using R32. *Int. J. Therm. Sci.* **2013**, *68*, 103–109. [[CrossRef](#)]
15. Xu, X.; Hwang, Y. Performance comparison of R410A and R32 in vapor injection cycles. *Int. J. Refrig.* **2013**, *36*, 892–903. [[CrossRef](#)]
16. Yu, J.; Song, X.; Ma, M. Theoretical study on a novel R32 refrigeration cycle with a two-stage suction ejector. *Int. J. Refrig.* **2013**, *36*, 166–172. [[CrossRef](#)]

17. Alabdulkarem, A.; Eldeeb, R.; Hwang, Y.; Aute, V.; Radermacher, R. Testing, simulation and soft-optimization of R410A low-GWP alternatives in heat pump system. Essai, simulation et optimisation légère des frigorigènes alternatifs à faible GWP au R410A dans un système de pompe à chaleur. *Int. J. Refrig.* **2015**, *60*, 106–117. [[CrossRef](#)]
18. In, S.; Cho, K.; Lim, B.; Lee, C. Partial load performance test of residential heat pump system with low-GWP refrigerants. *Appl. Therm. Eng.* **2015**, *85*, 179–187. [[CrossRef](#)]
19. Ma, S.; Hu, J.; Wang, X.; Ji, J. Effect of Non-Uniformity of Rotor Stagger Angle on the Stability of a Low-Speed Axial Compressor. *Energies* **2022**, *15*, 2714. [[CrossRef](#)]
20. Moreno, J.; Dodds, J.; Sheaf, C.; Zhao, F.; Vahdati, M. Aerodynamic Loading Considerations of Three-Shaft Engine Compression System During Surge. *J. Turbomach.* **2021**, *143*, 121002. [[CrossRef](#)]
21. Zhao, F.; Dodds, J.; Vahdati, M. Flow Physics during Surge and Recovery of a Multi-Stage High-Speed Compressor. *J. Turbomach.* **2021**, *84102*, V02ET41A009. [[CrossRef](#)]
22. Wang, R.; Yu, X.; Liu, B.; An, G. Effects of Loading Level on the Variation of Flow Losses in Subsonic Axial Compressors. *Energies* **2022**, *15*, 6251. [[CrossRef](#)]
23. An, G.; Fan, Z.; Qiu, Y.; Wang, R.; Yu, X.; Liu, B. Numerical Investigation of the Effect of Hub Gaps on the 3D Flows Inside the Stator of a Highly Loaded Axial Compressor Stage. *Energies* **2022**, *15*, 6993. [[CrossRef](#)]
24. Pantelidis, K.; Hall, C. Reynolds number effects on the aerodynamics of compact axial compressors. In Proceedings of the 12th European Conference on Turbomachinery Fluid Dynamics and Hermodynamics, Stockholm, Sweden, 3–7 April 2017; pp. 2410–4833.
25. Kim, T.G.; Jung, Y.J.; Jung, Y.; Choi, M. Effects of Low Reynolds Numbers on Performance of a One-Stage Axial Compressor. *Trans. Jpn. Soc. Aeronaut. Space Sci.* **2015**, *58*, 280–288. [[CrossRef](#)]
26. Hutchings, J.; Hall, C. The Effects of Reynolds Number on the Stall and Pre-Stall Behavior of Compact Axial Compressors. *J. Turbomach.* **2021**, *143*, 121014. [[CrossRef](#)]
27. Li, P.; Zuo, Z.; Zhou, X.; Li, J.; Chen, H. Investigation of different rotational speed characteristics of multistage axial compressor in caes system. *Energies* **2023**, *16*, 4383. [[CrossRef](#)]
28. Tu, B.; Zhang, X.; Hu, J.; Zhong, M.; Xiong, B. Analysis methods for aerodynamic instability detection on a multistage axial compressor. *J. Aerosp. Eng.* **2021**, *2021*, 8893792. [[CrossRef](#)]
29. Tu, B.; Zhang, X.; Hu, J. Experimental and numerical investigation on effects of the steam ingestion on the aerodynamic stability of an axial compressor. *Entropy* **2020**, *22*, 1416. [[CrossRef](#)]
30. Vuong, T.; Kim, K. Stability enhancement of a single-stage transonic axial compressor using inclined oblique slots. *Energies* **2021**, *14*, 2346. [[CrossRef](#)]
31. Huang, S.; Yang, C.; Wang, M.; Zhao, S.; Lu, X. The influence of backward sweep on aerodynamic performance of a 1.5-stage highly loaded axial compressor. In Proceedings of the Global Power and Propulsion Society, Beijing, China, 16–18 September 2019.
32. Guang, W.; Chu, W.; Zhang, H.; Guo, Z. Mechanism of Affecting the Performance and Stability of an Axial Flow Compressor with Inlet Distortion. *J. Therm. Sci.* **2021**, *236*, 2031–2043.
33. Kumar, S.S.; Kumar, L.; Kumaran, R.S.; Kumar, V.S.; Shobhavathy, M. Design of high transonic axial compressor stage for small gas turbine applications. In *Gas Turbine India Conference*; American Society of Mechanical Engineers: Houston, TX, USA, 2019.
34. Danish, S.N.; Qureshi, S.R.; Imran, M.M.; Khan, S.U.D.; Sarfraz, M.M.; El-Leathy, A.; Al-Ansary, H.; Wei, M. Effect of tip clearance and rotor–stator axial gap on the efficiency of a multistage compressor. *Appl. Therm. Eng.* **2016**, *99*, 988–995. [[CrossRef](#)]
35. Schulze, W.M.; Erwin, J.R.; Ashby, G.C. NACA 65-series compressor rotor performance with varying annulus-area ratio, solidity, blade angle, and Reynolds number and comparison with cascade results. In *Technical Note 4130*; Langley Aeronautical Laboratory: Hampton, VA, USA, 1957.
36. Wu, X.; Liu, B.; Ricks, N.; Ghorbaniasl, G. Surrogate Models for Performance Prediction of Axial Compressors Using through-Flow Approach. *Energies* **2020**, *13*, 169. [[CrossRef](#)]
37. Zhao, W.; Zheng, Q.; Jiang, B.; Lin, A. A Passive Control Method of Hub Corner Stall in a 1.5-Stage Axial Compressor under Low-Speed Conditions. *Energies* **2020**, *13*, 2691. [[CrossRef](#)]
38. Lieblein, S. Experimental flow in two-dimensional cascades. In *Aerodynamic Design of Axial-Flow Compressors—Revised*; Johnsen, I.A., Bullock, R.O., Eds.; National Aeronautics And Space Administration: Washington, DC, USA, 1965; pp. 32–58.
39. ANSYS. *Ansys ©Research Turbogrid and Ansys ©Research Fluent*; Release 24.2; Theory Guide; ANSYS, Inc.: Canonsburg, PA, USA, 2024.
40. Menter, F.R. Two-equation eddy-viscosity turbulence models for engineering applications. *AIAA J.* **1994**, *32*, 1598–1605. [[CrossRef](#)]
41. Yan, W.; Sun, Z.; Zhou, J.; Zhang, K.; Wang, J.; Tian, X.; Tian, J. Numerical simulation of transonic compressors with different turbulence models. *Aerospace* **2023**, *10*, 784. [[CrossRef](#)]
42. Shi, X.; Liu, H.; Long, F.; Tang, J.; Wang, L. Study on the influence of blade roughness on axial flow compressor stage performance. *MATEC Web Conf.* **2017**, *108*, 08008. [[CrossRef](#)]

43. Moreno, J.M.D.; Dodds, J.A.; Vahdati, M.; Stapelfeldt, S. Deficiencies in turbulence modelling for the prediction of the stability boundary in highly loaded compressors. In *Turbo Expo: Power for Land, Sea, and Air*; American Society of Mechanical Engineers: Houston, TX, USA, 2019 ; Volume 58554, p. V02AT39A025.
44. Sinnette, J.T. Analysis of Effect of Basic Design Variables on Subsonic Axial-Flow-Compressor Performance. In *NACA Report 90*; Langley Aeronautical Laboratory: Hampton, VA, USA, 1948

Disclaimer/Publisher’s Note: The statements, opinions and data contained in all publications are solely those of the individual author(s) and contributor(s) and not of MDPI and/or the editor(s). MDPI and/or the editor(s) disclaim responsibility for any injury to people or property resulting from any ideas, methods, instructions or products referred to in the content.